EXPERIMENTAL INVESTIGATION OF LIQUID METAL EMULSION EFFECT ON THE HEAT TRANSFER PERFORMANCE OF AN OSCILLATING HEAT PIPE

A Thesis

Presented to

the Faculty of the Graduate School

at the University of Missouri – Columbia

In Partial Fulfillment

of the Requirements for the Degree

Master of Science

---

by

MARK OWOOLA

Professor Hongbin Ma, Advisor and Thesis Supervisor

MAY 2022

The undersigned have examined the thesis entitled

EXPERIMENTAL INVESTIGATION OF LIQUID METAL EMULSION EFFECT ON THE HEAT TRANSFER PERFOMANCE OF AN OSCILLATING HEAT PIPE

presented by Mark Owoola

a candidate for the degree of

Master of Science Mechanical & Aerospace Engineering

and hereby certify that in their opinion it is worthy of acceptance.

_____

Professor Hongbin Ma

_____

Professor Gary Solbrekken

_____

Professor Stephen Montgomery-Smith

Acknowledgements

Thank you, Mom, and Dad, for your unconditional and unending love and support. You both have been shining examples of what it means to put my best effort into everything I do, and to aim higher than what I believe the limits of my capabilities are.

Thank you to my dearest siblings, Michael, and Miriam. I will always work hard to be the role model you both deserve.

I give my thanks to Professor Hongbin Ma, my thesis supervisor and research sponsor, for his constant guidance, support, and encouragement over the past two years. You have ignited a passion for research in me, and I hope to carry and cultivate that spirit of discovery for the rest of my life.

I would also like to give my sincere thanks to my colleagues for enthusiastically lending me their knowledge and support:

Adalberto Aviles

Dr. Shahabeddin Mohammadian

Dr. Laith Ismael

Jeremy Spitzenberger

Table of Contents

Nomenclature

A	Area [m^2]
C	Fraction coefficient
D	Diameter [m]
d	Distance [m]
E	Energy [J]
h	Heat transfer coefficient [W/m^2-°C]
k	Thermal conductivity [W/m-°C]
g	Gravitational constant [m/s^2]
I	Current [A]
OHP	Oscillating heat pipe
P	Pressure [Pa]
R	Thermal Resistance [°C/W]
T	Temperature [°C]
u	Velocity [m/s]
Q	Thermal energy [W]

Greek

Δ	Increment
∂	Partial differential
μ	Viscosity [Pa-s]
ρ	Density [kg/m^3]
σ	Surface tension [N/m]
ϕ	Volume fraction

Subscripts

c	Condenser
crit	Critical
e	Evaporator
eff	Effective
f	Fluid
i	Interface
l	Liquid
loss	Loss
s	Solid
sat	Saturation
t	Thickness
v	Vapor

List of Tables

List of Figures

Abstract

This thesis introduces an oscillating heat pipe (OHP) charged with a hybrid fluid of gallium and ethanol. The hybrid fluid is fabricated using an ultrasonication technique to produce an emulsion-based mixture of liquid metal gallium microdroplets suspended in an ethanol solution. The hybrid fluid OHP is modelled and numerically simulated in ANSYS Fluent using the volume of fluid (VOF) technique to analyze its startup behavior, steady-state oscillatory flow, and heat transfer performance. The heat transfer performance of the OHP is investigated experimentally with different mass concentrations of gallium at a 50% filling ratio. The OHP is fabricated from a copper plate and contains a six-turn channel with a 3×3 mm^2 cross-section. Steady-state oscillating motion is achieved with weight concentrations of gallium up to 20%. The experimental results show that using gallium-in-ethanol hybrid fluid emulsion as the working fluid can increase the heat transfer of the OHP by up to 7.8% over pure ethanol at 300 W.

Chapter I. Introduction

As modern technologies require higher power demands, increasing attention to the development and improvement of thermal management technologies is necessary to eliminate increasing heat fluxes. The exponential rise of computing power paired with a continuous reduction in the size of hardware components has resulted in high heat densities. The high temperatures generated pose major risks to the structure, lifetime, and performance of these hardware components. This hazard is magnified in space applications, as space vehicles face extremely high heat loads upon launch, reentry, and in outer space. Heat pipes have great potential to address these thermal management challenges.

A heat pipe, as seen in Fig. 1.1, is a heat transfer device consisting of a sealed container with a working fluid inside. The heat pipe exchanges heat using a combination of conduction, convection, and phase-change heat transfer. Heat from a heat source is transferred to the outer material of a heat pipe through conduction. The working fluid inside the heat pipe then absorbs this heat and evaporates. The area where this occurs is referred to as the ‘evaporator section’ of the heat pipe. The gas is pushed by the pressure difference produced through the ‘adiabatic section’ to a lower temperature region, called the ‘condenser section’. Condensation occurs at this point, releasing the heat to the outer material of the heat pipe, which is then conducted away by the heat sink. In conventional heat pipes, the heat transfer cycle is repeated by using forces such as gravity or the capillary force induced by an internal wick structure to push the condensed fluid back into the evaporator section. Heat pipes can operate over a wide temperature range, from the freezing to critical points of the working fluid. Heat pipes are also passive devices, meaning they

do not output work externally or take inputted work to operate. The synthesis of conductive, convective, and phase-change heat transfer makes the heat pipe a very effective heat dissipation device. However, as heat fluxes continue to increase rapidly, conventional heat pipes are no longer adequate in transporting away the additional heat.

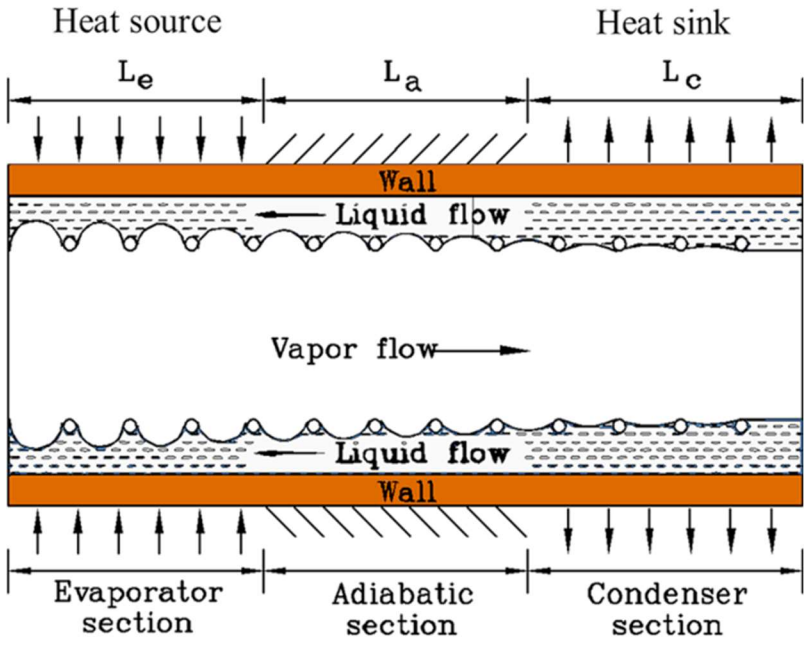

Figure 1.1 Schematic of a conventional heat pipe

The oscillating heat pipe (OHP), as seen in Fig 1.2, uses pressure driven oscillatory flow in addition to conduction, convection, and phase-change heat transfer, to effectively transport heat [1,2]. An OHP consists of connected, serpentine-like channels or tubes that are small enough in diameter for the working fluid inside to separate into a train of alternating liquid plugs and vapor slugs. Similar to a conventional heat pipe, heat is absorbed from the heat source in the evaporator section. The working fluid absorbs this heat and undergoes evaporation, expanding the volume and increasing the pressure of the vapor slugs. Heat is rejected into the heat sink via the condenser section. The condensation of the working fluid in this section results in the contraction of volume and reduction of pressure of the vapor slugs. The pressure imbalances caused by the expansion and

contraction of the vapor slugs produces the driving force that oscillates the liquid plugs. OHPs hold numerous advantages over conventional heat pipes. As opposed to conventional heat pipes, the working fluid in an OHP is thermally driven, voiding the need for an internal wick structure to facilitate capillary flow. Due to this lack of internal wick structure, OHPs can be readily manufactured into different shapes and sizes, from flat-plate OHPs to U-shaped OHPs [3].

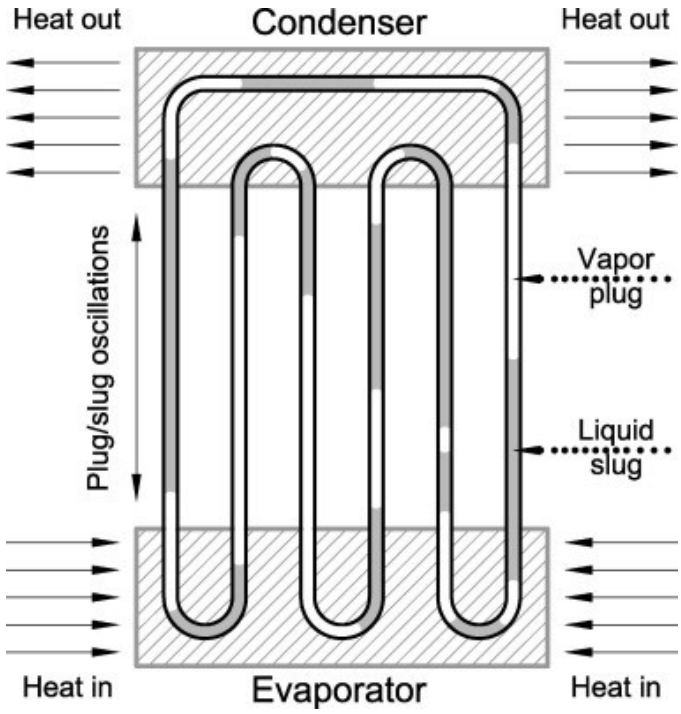

Figure 1.2 Schematic of an oscillating heat pipe

Experimental investigations have determined that the material selection, physical dimensions, and working fluid selection of an OHP significantly affect overall heat transfer performance. Intermolecular interactions between the working fluid and the channel/tube material of an OHP determine important properties like wettability and fluid flow resistance, influencing the oscillatory behavior and heat transfer capability of the working fluid [4]. For example, OHPs fabricated from base materials with hydrophilic surfaces have been shown to reduce fluid flow resistance and therefore increase liquid plug movement

and heat transfer [5,6]. Other physical properties such as the effective channel inner diameter and filling ratio of the OHP, the thermal conductivity, viscosity, and latent heat of fusion of the working fluid have been shown to influence the overall performance of an OHP according to previous research. Working fluids with a high $(\frac{dP}{dT})_{sat}$, the slope of the vapor-liquid coexistence curve, and a low latent heat have been shown to improve the start-up performance of OHPs [7,8]. A low latent heat allows for the fluid to quickly evaporate and condensate with relatively little heat input. A steep slope of the vapor-liquid saturation line means that small changes in temperature result in high pressure changes when the fluid is in a saturated state. These properties enable a high driving force of the liquid plugs. However, low latent heat fluids have a drawback of having relatively low thermal conductivities. A high thermal conductivity of both the OHP material and working fluid is an important factor in good performance because the rate of heat transfer through a substance is directly proportional to its thermal conductivity. More so, conduction is one of the main mechanisms of transferring sensible heat, which accounts for between 80 and 90% of the total energy transferred by OHPs [9].

Liquid metals have been investigated [10,11] as a novel working fluid in thermal management devices because they contain the properties of both a fluid and a metal. Liquid metals are a unique class of metals that exist in a liquid state at or around room temperature. In addition to their fluidity, liquid metals retain the high thermal conductivity that most metals have. However, liquid metals cannot be the sole working fluid in closed loop OHPs. Heat transfer devices that use pure liquid metal need an external energy source, such as a magnetohydrodynamic (MHD) pump, to provide the necessary driving force for operation. For use in closed loop OHPs, a liquid metal needs to be supplemented with a phase change

fluid that can provide the driving force needed for the OHP to operate without an external energy source. This pairing of liquid metal with a phase change fluid is known as a liquid metal hybrid fluid. Previous research has shown that a liquid metal hybrid fluid of water and galinstan can improve the heat transfer performance of an OHP under certain conditions [12]. Hao et al. [12] tested hybrid fluids of varying concentrations in an OHP under varying heat loads. It was found that the hybrid fluid of galinstan and water improved the thermal performance of an OHP at higher inputs between 260 and 420 W. The hybrid fluid OHP performed worse than the OHP charged with pure water at all heat loads under 260 W. In addition, increasing the concentration of galinstan required a higher heat input to start up oscillatory behavior and only benefited the heat transfer capability of the OHP at heat inputs above 260 W. Galinstan is an alloy of gallium with a thermal conductivity of 16.5 W/m·K, which is 27 times higher than that of water. It exists in a liquid state at room temperature and is non-toxic. These qualities make gallium and its alloys an ideal working fluid for an efficient cooling device. However, galinstan has a relatively high density and viscosity, 6.45 and 2.4 times greater than water respectively. Due to this, large concentrations of liquid metal can slow down the oscillation of the hybrid fluid and negatively affect the overall performance of an OHP.

Nanoparticles that are suspended in base fluids, known as nanofluids, both increase the thermal conductivity of the working fluid and reduce the effective thermal resistance of an OHP significantly with concentrations of less than 1 wt.% [13,14]. The emulsion of liquid metal in a base fluid can be seen as similar structurally to a nanofluid, with micro-sized dispersed liquid metal droplets being suspended in a continuous fluid. Previous studies have investigated the heat transfer of liquid-liquid emulsions. Kumano et al. [15]

found that heat transfer was enhanced using an emulsion of high viscosity oil as compared to low viscosity oil and water. Studying the heat transfer of an Ethanol/Polyalphaolefin (PAO) nanoemulsion flowing through a microchannel, Trinh et al. [16] found an up to 70% increase in the heat transfer coefficient compared to pure PAO under flow boiling conditions. Further research is needed however, because the mechanisms behind improved heat transfer of liquid-liquid emulsions are not yet fully understood.

Most of the research concerning OHPs have been experimental in nature because of the difficulty of modelling complex two-phase systems. Predicting the thermal performance of potential OHP configurations is important to ensure they are optimized for use in their areas of application. The monetary and time associated costs of performing large amounts of physical experiments is not economically viable, so the use of numerical simulations is important for future OHP research. The predominant flow regime found inside OHPs is slug flow. Slug flow is a two-phase flow regime characterized by an alternating sequence of vapor plugs and liquid slugs. Numerous investigations have endeavored to numerically model the behavior of this kind of flow inside capillary tubes and oscillating heat pipes. Smoot et al. [17] developed a two-phase model of slug flow using the volume of fluid method. A bias factor was used to increase the mesh resolution near the wall boundaries to capture the thin film region. The effect of oscillation on the fluid flow inside a capillary channel and the wall sheer stresses were analyzed. Taha et al. [18] simulated the motion of a Taylor bubble (vapor plug) rising in a vertical column of flowing liquid inside a tube with a circular cross-section. The volume of fluid (VOF) method was used in the commercial CFD package ANSYS Fluent. The bubble shape and velocity profiles along with the velocity flow field were determined under different

capillary numbers. The results compared well with experimental investigations. Liu et al. [19] numerically investigated the phase-change and mass transfer process of a closed loop oscillating heat pipe (CLOHP) using the VOF method. The model successfully simulated the complex flow patterns of the CLOHP, such as alternating slug flow and annular flow, under different operating conditions.

In this investigation, the effect of liquid metal in phase-change fluid emulsions on the heat transfer performance of an OHP is analyzed numerically and experimentally. The CFD package ANSYS Fluent is utilized to analyze the heat transfer performance of an OHP. Gallium microdroplets are fabricated using an ultrasonication process and mixed into solutions of varying concentrations with ethanol. An experimental setup is developed for the emulsion-based hybrid fluid OHP (HFOHP), which is tested against an OHP using pure ethanol as its working fluid. Variables such as heat transfer coefficient, h, thermal resistance, R, and effective thermal conductivity, k_{eff}, are calculated. An analysis of the experimental data is conducted to compare with the numerical results and to determine whether using gallium-in-ethanol emulsion hybrid fluid improves the heat transfer performance over using pure ethanol and reduces the amount of gallium needed to enhance heat transfer compared to previous research.

Chapter II. Numerical Analysis with ANSYS FLUENT

2.1 Volume of Fluid (VOF) Method

The volume of fluid (VOF) method is a numerical technique used in computational fluid dynamics that utilizes a fraction function, C, to track the volume fraction of every cell in a computational grid, as seen in Fig. 2.1. This allows for the modelling of two or more immiscible fluids by solving only a single set of momentum equations, making this method computationally friendly. Through tracking the free surface, or liquid-vapor interface, the VOF method can predict the complex dynamics of two-phase systems, such as the motion of a bubble inside a liquid.

Figure 2.1 Schematic description of VOF method

To track the liquid-vapor interface, the fraction coefficient, C, is incorporated into the continuity equation, i.e.,

$$\frac{\partial C_m}{\partial t} + \boldsymbol{u} \cdot \nabla C_m = 0 \tag{2.1.1}$$

with the constraint being

$$\sum_{m=1}^{n} C_m = 1 \tag{2.1.2}$$

C_m will equal zero inside of a cell that is empty of the m_{th} fluid and will equal one when it is full. Cells located at the liquid-vapor interface will have a value between zero and one. Properties that appear in the momentum and energy transport equations, such as density, ρ, viscosity, μ, and effective thermal conductivity, k, are volume-averaged accordingly, i.e.,

$$\rho = \sum_{m=1}^{n} C_m \rho_m \tag{2.1.3}$$

$$\mu = \sum_{m=1}^{n} C_m \mu_m \tag{2.1.4}$$

$$k_{eff} = \sum_{m=1}^{n} C_m k_m \tag{2.1.5}$$

Density, viscosity, and effective thermal conductivity are incorporated into momentum and energy transfer equations respectively, i.e.,

$$\frac{\partial}{\partial t}(\rho \boldsymbol{u}) + \nabla \cdot (\rho \boldsymbol{u}^2) = -\nabla p + \nabla \cdot \left[\mu\left(\nabla \boldsymbol{u} + \nabla \boldsymbol{u}^{\mathrm{T}}\right)\right] + \rho g + \boldsymbol{F} \tag{2.1.6}$$

$$\frac{\partial}{\partial t}(\rho E) + \nabla \cdot (\boldsymbol{u}(\rho E + p)) = \nabla \cdot \left(k_{eff} \nabla T\right) \tag{2.1.7}$$

where **u** is the velocity vector, **g** is the gravitational constant, p is the pressure, and E is the energy.

2.2 Simulation Setup

A 2D model of the fluid carrying channels within the OHP, as seen in Fig. 2.2 is created in Ansys SpaceClaim, a multipurpose modelling tool. The channel dimensions are set equal to those of the OHP used in the experimental investigation: channel width of 3 mm, six turns, and 107 mm long from the bottom of the evaporator section to the top of the condenser section. The model is divided into eight separate groups: evaporator, adiabatic bottom, adiabatic top, condenser, evaporator wall, adiabatic bottom wall, adiabatic top wall, and condenser wall. These groups allow for boundary and internal conditions to be set once the model is exported to Ansys Fluent.

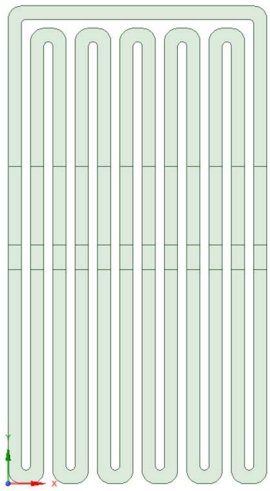

Figure 2.2 2D model of OHP created in Ansys SpaceClaim

This model is then imported into the meshing tool where it is discretized into a 2D mesh, as shown in Fig. 2.3. The mesh element size is set to 0.35 mm, with the behavior set to hard to ensure uniform meshing across the model.

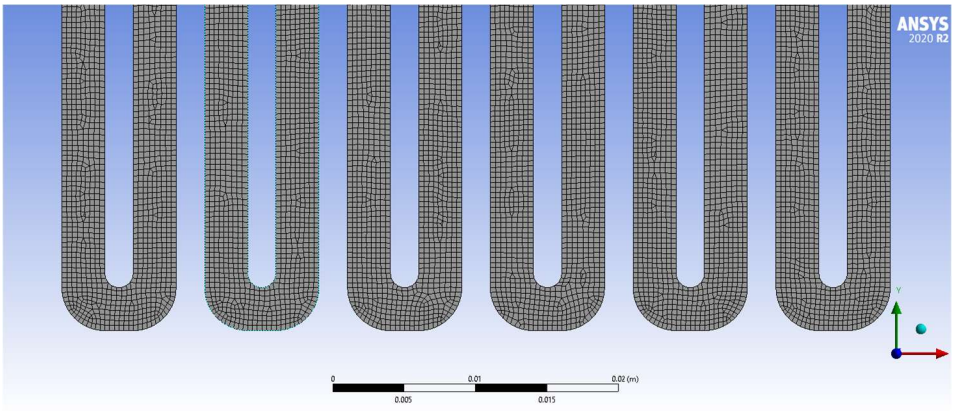

Figure 2.3 2D Mesh

After the mesh has been created, it is opened in Ansys Fluent, where the necessary initial conditions are defined for the simulation. Fluent contains two techniques for modelling two-phase flow, the mixture method, and the volume of fluid (VOF) method. The VOF method is chosen for this investigation because of its computational efficiency. The bottom half of the OHP is set to contain pure liquid and the top half is set to contain pure vapor as the initial condition, as seen in Fig. 2.4. Pure ethanol is used as the working fluid along with 5%, 10%, and 20% gallium-in-ethanol emulsions. The emulsions are modelled using the effective density, ρ_{eff}, and effective thermal conductivity, k_{eff}, of each emulsion. The effective density of the working fluid are calculated by

$$\rho_{eff} = \frac{\rho_l \rho_s}{(1-w)\rho_s + w\rho_l} \tag{2.1.8}$$

To determine the theoretical effective thermal conductivity of the resulting hybrid fluid, the model derived by Krupiczka et al. [20] is used

$$k_{eff} = k_l \left(\frac{k_s}{k_l}\right)^{0.28 - 0.757\log(\phi) - 0.057\log\left(\frac{k_s}{k_l}\right)} \tag{2.1.9}$$

where k_l is the thermal conductivity of the continuous phase fluid, k_s is the thermal conductivity of the solid particle, and ϕ is the volume-based void fraction. The gallium microdroplets are treated as solid particles because of their high density and surface tension

compared to ethanol. For any concentration gallium-in-ethanol emulsion, the volume-based void fraction can be expressed as

$$\phi = \frac{(1-\omega)\rho_s}{(1-\omega)\rho_s + \omega\rho_f} \tag{2.1.10}$$

where ρ_l is the density of liquid ethanol, ρ_s is the density of gallium, and ϕ is the volume fraction. All other properties are based on a pure ethanol solution.

Three temperature differences between the condenser wall and evaporator wall are simulated: 20-40 °C, 40-70 °C, and 60-100 °C. The adiabatic wall is set to a zero heat flux condition. As seen in Fig. 2.4, the bottom half of the OHP is initially set to be 100% liquid and the top half to be 100% vapor. The simulations are run for 20000 time-steps with each time step being 0.00075 s, resulting in 15 second simulations. Volume fraction, temperature, and heat transfer coefficient data are analyzed in order to better understand the two-phase flow and heat transfer mechanisms of the OHP.

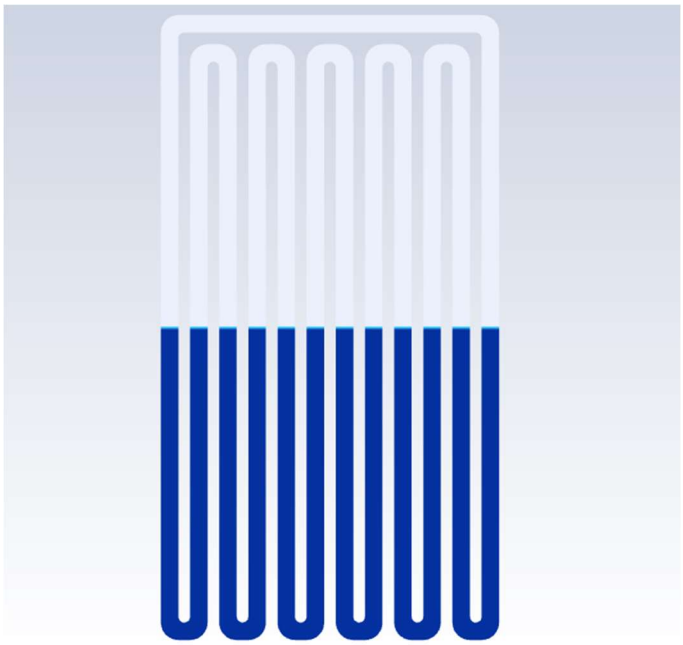

Figure 2.4 Initial condition of OHP: liquid (blue), vapor (white)

2.3 Simulation Results

The numerical model successfully captures the oscillatory behavior of the OHP. Oscillation is obtained under all temperature differences and gallium concentrations. Immediately after the simulation starts, mixing of the liquid and vapor occurs at the original liquid-vapor interface. A film of condensate then begins to grow inwards from the walls of the condenser section while small vapor bubbles form on the walls of the evaporator section. The bubbles grow until they coalesce into vapor plugs, pushing the liquid column of water above them as they rise into the condenser. Further separation inter liquid slugs and vapor plugs occurs past this point and oscillation begins to occur in a steady manner. Figure 2.5 shows the startup behavior of the OHP charged with pure ethanol with a 40 °C temperature difference between the evaporator and condenser walls. A darker blue indicates a higher liquid volume fraction.

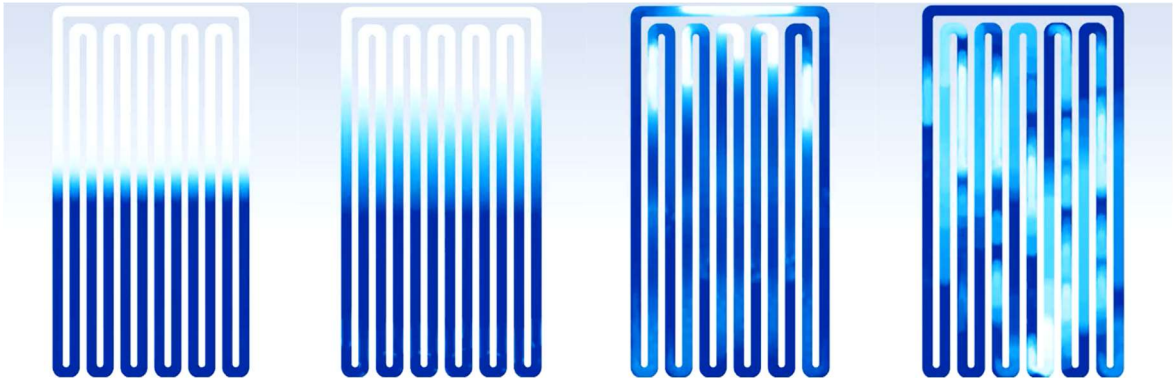

Figure 2.5 Start-up behavior of OHP (volume fraction)

Figure 2.6 shows the temperature variation across the working fluid as it undergoes steady oscillation. The working fluid is ethanol with a 40 °C temperature difference between the evaporator and condenser walls. The cycle starts in Fig. 2.6 (a) with colder fluid in the evaporator and warmer fluid in the condenser. Fig. 2.6 (b) and (c) show the resultant temperature increase of the fluid in the evaporator and the temperature drop of

the fluid in the condenser. Fig. 2.6 (d) shows the colder fluid flowing down back into the evaporator and the warmer fluid rising, completing the cycle.

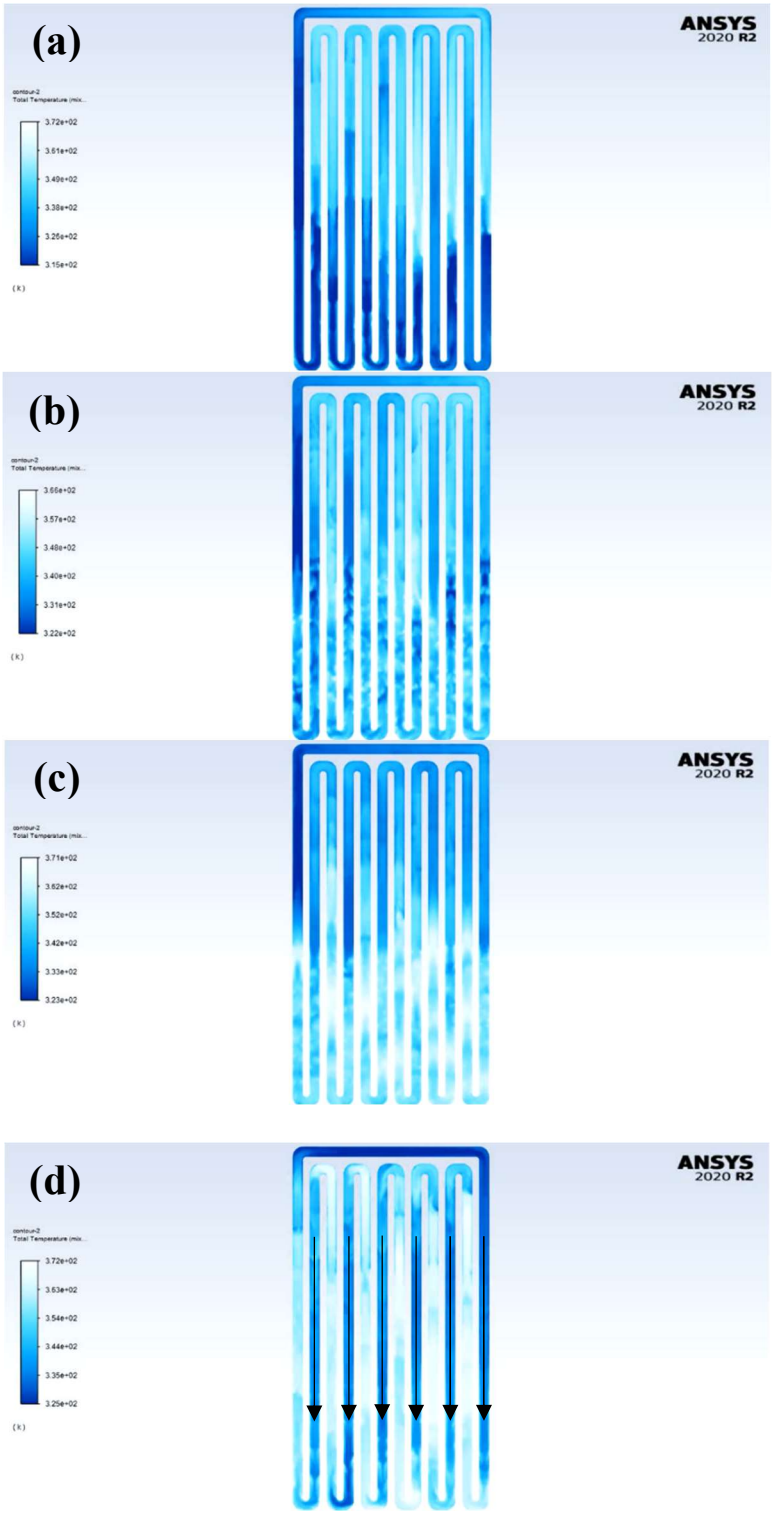

Figure 2.6 (a)-(b) Temperature distribution of working fluid during oscillation

In Ansys Fluent, the heat transfer coefficient, h, is calculated using the heat flux, reference temperature, and the wall temperature. The reference temperature can either be user defined, as it is when the surface heat transfer coefficient option is used, or it can be calculated using the nearest cell centroid temperature, as it is when wall function heat transfer coefficient is used. For this investigation, the wall function heat transfer coefficient is used. However, Fluent does not take into consideration the heat transfer due to phase change when calculating for the heat transfer coefficient. It has already been established that between 80 and 90% of the heat transferred in an oscillating heat pipe is due to sensible heat [9]. Since conduction and convection are the main drivers of sensible heat transfer, an assumption can be made that these two heat transfer mechanisms will have an order of magnitude higher effect on the value of the heat transfer coefficient than the effect of phase change. Therefore, the change in the value of the heat transfer coefficient across the different emulsions in the simulation will be a good indicator for the gallium concentration effect on the OHPs heat transfer performance during physical experimentation.

The heat transfer results of the simulations are seen in Fig. 2.7, where the wall function heat transfer coefficient, h, is plotted against the temperature difference between the evaporator and condenser, ΔT. Using ethanol as the working fluid, the heat transfer coefficient goes up slightly as ΔT increases from 20 to 40 °C, changing from 735 W/m2-K to 859 W/m2-K. All the emulsions have a slight upward trend as ΔT increases from 20 to 40 °C. At ΔT= 20 °C, the 20% wt. emulsion performs outperforms the ethanol control and the other emulsions, achieving a wall function heat transfer coefficient of 1814 W/m2-K. The 5% wt. and 10% wt. emulsions achieve a wall function heat transfer coefficient of 1605 W/m2-K and 1459 W/m2-K respectively. When ΔT= 40 °C, no significant difference

in heat transfer performance is found between the emulsions. Across all temperature ranges, implementing the emulsions approximately doubles the wall function heat transfer coefficient as compared to using ethanol.

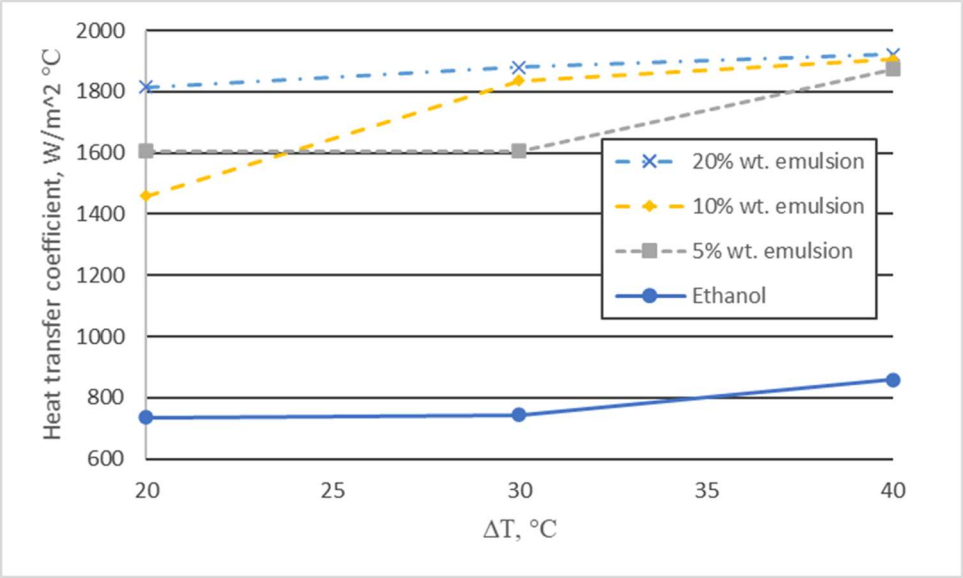

Figure 2.7 Heat transfer coefficient vs. ΔT (Fluent)

Figure 2.8 shows the thermal resistances found inside an OHP. In pathway A, the heat is transferred across the copper shell and interface in the evaporator, through the working fluid, and back across the interface and shell in the condenser. $R_{t,e/c}$ is the resistance of the shell due to its thickness, $R_{i,e/c}$ is the resistance of the shell/fluid interface, and R_f is the resistance of the working fluid. In pathway B, the heat is transferred along the length of the shell and encounters the resistance, R_{Leff}. The resistances of the two paths can be idealized as being parallel to each other. The theoretical effective thermal conductivity of the OHP can be expressed as

$$k_{eff} = \frac{L_{eff}}{AR_T} \tag{2.3.1}$$

where L_{eff} is the effective length of the OHP, A is the cross-sectional area, and R_T is the total thermal resistance. R_T can be expressed as

$$R_T = \frac{R_A R_B}{R_A + R_B} \tag{2.3.2}$$

where R_A is

$$R_A = R_{t,e} + R_{i,e} + R_f + R_{t,c} + R_{i,c} \tag{2.3.3}$$

and R_B is

$$R_B = R_{Leff} \tag{2.3.4}$$

The thermal resistance of the shell's thickness can be calculated by

$$R_{t,e/c} = \frac{t}{k_{Cu} A_{s,e/c}} \tag{2.3.5}$$

where t is the shell thickness, k_{Cu} the thermal conductivity of copper, and $A_{s,e/c}$is the area of the evaporator or condenser. The interface thermal resistance can be calculated by

$$R_{i,e/c} = \frac{1}{hA_{h,e/c}} \tag{2.3.6}$$

where h is the heat transfer coefficient and $A_{h,e/c}$ are the surface areas of the channels in the evaporator and condenser sections of the OHP. The thermal resistance of the shell's length can be calculated by

$$R_{Leff} = \frac{L_{eff}}{k_{Cu} A} \tag{2.3.7}$$

The thermal resistance of the working fluid is assumed to equal zero. Using the values of the wall flux heat transfer coefficient calculated by Fluent for h, the theoretical effective thermal conductivity of the OHP can be found. Table 2.1 shows the theoretical effective thermal conductivity of the OHP charged with varying emulsion concentrations.

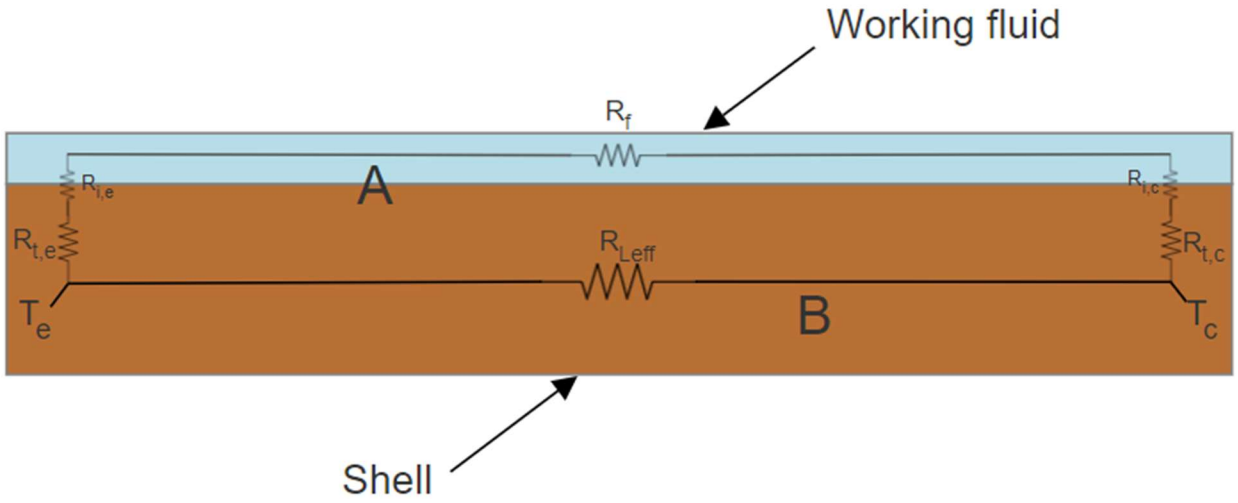

Figure 2.8 Thermal resistance diagram of OHP

Table 2.1 Theoretical effective thermal conductivity of OHP

Working Fluid	**ΔT [°C]**	**Theoretical k_{eff} [W/m-°C]**
Ethanol	20	543.9
	30	545.8
	40	571.7
5% wt. emulsion	20	726.3
	30	727.1
	40	783.3
10% wt. emulsion	20	694.5
	30	773.1
	40	788.4
20% wt. emulsion	20	770.1
	30	783.3
	40	791.6

Chapter III. Fabrication of Hybrid Fluid

3.1 Thermophysical Properties of Ethanol and Gallium

Gallium is a liquid metal, one of five naturally occurring liquid metals, i.e., a metal that exists in a liquid state around room temperature. Gallium has a useful synthesis of properties that are similar to both a liquid and a metal. Gallium is also non-toxic, in contrast to other liquid metals like mercury. Due to this, gallium has been chosen as the liquid metal for this work and is a strong candidate for use in further experimentation of OHPs. As a pure gallium OHP would require an external driving force to operate, a phase-change fluid needs to be implemented for a self-actuating OHP device to be feasible. The performance of ethanol has been studied in previous research in comparison to other working fluids, like water and acetone. Ethanol's low boiling point, density, and low latent heat of vaporization makes it a promising candidate for a phase-change fluid that can provide a driving force strong enough to oscillate the gallium. Table 1 shows the relevant physical properties of gallium and ethanol.

Table 3.1 Thermophysical properties of ethanol and gallium

Properties	Ethanol	Gallium
Density/kg·m^{-3}	789.2 at 20 ℃	6095 at 29 ℃
Melting Point/℃	-114.1 ℃ at 1 atm	29 ℃ at 1 atm
Boiling Point/℃	78.37℃ at 1 atm	2400 ℃ at 1 atm
Thermal Conductivity/W·m^{-1}℃$^{-1}$	0.167 at 50 ℃	29
Specific Heat/kJ·kg^{-1}℃$^{-1}$	2.561 at 25 ℃	0.370
Viscosity/Pa·s	0.001095 at 27 ℃	0.00137 at 77 ℃
Vapor Pressure/mmHg	44.6 at 20 ℃	1.53×10^{-7} at 906 ℃
Latent Heat of Vaporization/kJ·kg^{-1}	846	3671.8
Thermal Diffusivity/m^2·s^{-1}	8.27×10^{-8} at 25 ℃	1.29×10^{-5}

3.2 Ultrasonication Process

Finding efficient ways to create liquid metal microdroplets quickly in sufficiently large amounts has been a recent area of interest. Other than for heat transfer applications, gallium microdroplets have been suggested for use in flexible electronics, composites, and creating 3D structures [21]. Techniques for creating these microdroplets such as ultrasonication, flow-focusing microfluidics, and submerged electrodispersion have been studied and fine-tuned [21-23]. In this work, ultrasonication has been chosen as the method of choice due to its ability to produce gallium microdroplets in bulk and the wide range of working fluids that can be used as the continuous phase. Ultrasonication is the process of irradiating a liquid sample with sound waves of frequencies less than 20 kHz in order to agitate particles in the sample. These high energy waves create small vacuum pockets in the fluid, which then collapse on themselves and generate shockwaves. This phenomenon is called “cavitation” and is able to generate enough force to break up particles immersed in the fluid into smaller pieces. Liquid-liquid emulsions, where a dispersed phase fluid is suspended uniformly in another continuous phase liquid, can readily be produced using this technique.

A Cole-Parmer Ultrasonic Cleaner, seen in Fig 3.1, is used to create the gallium microdroplets in the ethanol solution. The water bath inside the device is warmed to 50 ℃ before containers containing different weight concentrations of gallium and ethanol are placed inside. The weight concentrations of gallium are 1%, 5% 10%, and 20%. The samples are then exposed to ultrasonic sound waves with a frequency of 40 KHz for 70 minutes. Figure 3.2 shows the resulting gallium-in-ethanol emulsions after the ultrasonication bath. As seen, the gallium is uniformly dispersed in the ethanol in the form

of microdroplets. Though the gallium microdroplets almost immediately begin to sediment to the bottom of the container, when given a light shake, they can be readily dispersed back into the solution of ethanol. This means that the gallium microdroplets will not coalesce back together and have formed permanent particles.

Figure 3.1 Cole-Parmer Ultrasonic Cleaner

Figure 3.2 From left to right: 5% wt., 10% wt., and 20% wt. gallium-in-ethanol emulsions

3.3 Analysis of Gallium-in-Ethanol Emulsion

Figure 3.3 shows a sample of the gallium microparticles viewed from a Nikon Eclipse LV150 with a M-10x microscope objective, providing a 100x magnification. The gallium particles are polydisperse, ranging in size from ~1 to 50 microns in diameter. Using ImageJ, the particle radius distribution of a sample of the gallium microdroplets is determined. Over 80% of the 2425 gallium microdroplets analyzed are under 2 microns in radius, and the average diameter is found 3 microns. Figure 3.4 shows the results of the analysis.

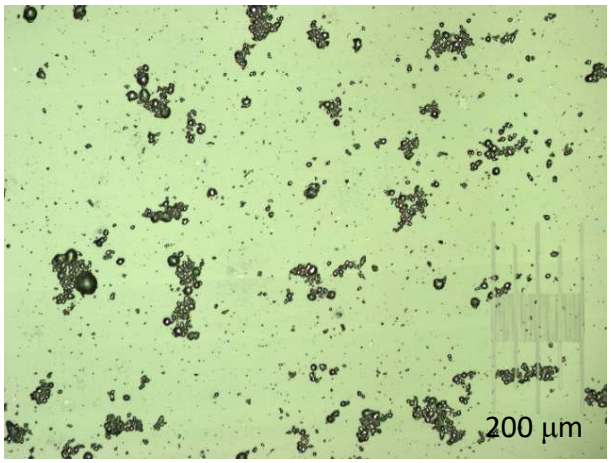

Figure 3.3 Gallium microparticles (left) and 1 mm calibration scale (right)

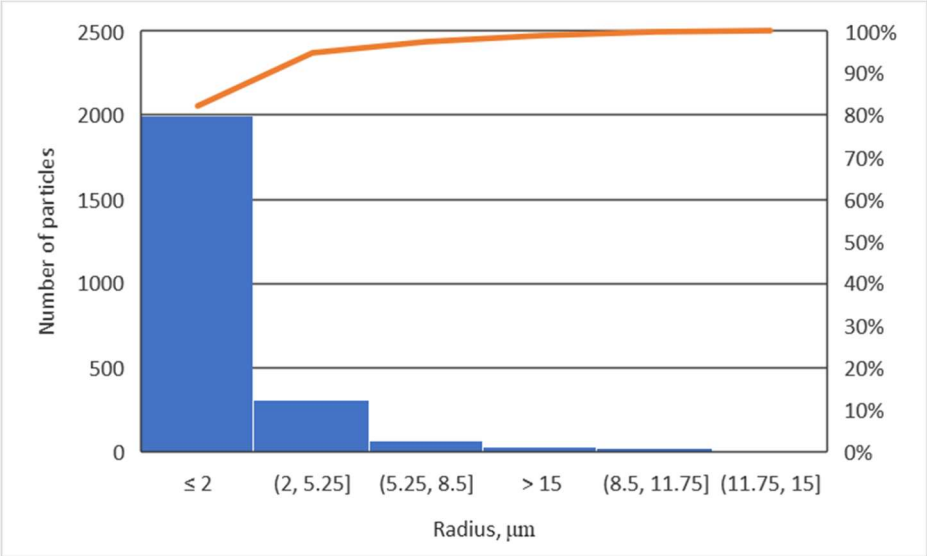

Figure 3.4 Radius distribution of a sample of gallium microparticles

Using Krupizcka's relation [20], the theoretical relationship between the mass fraction of gallium and the effective thermal conductivity of the hybrid fluid is shown in Figure 3.5.

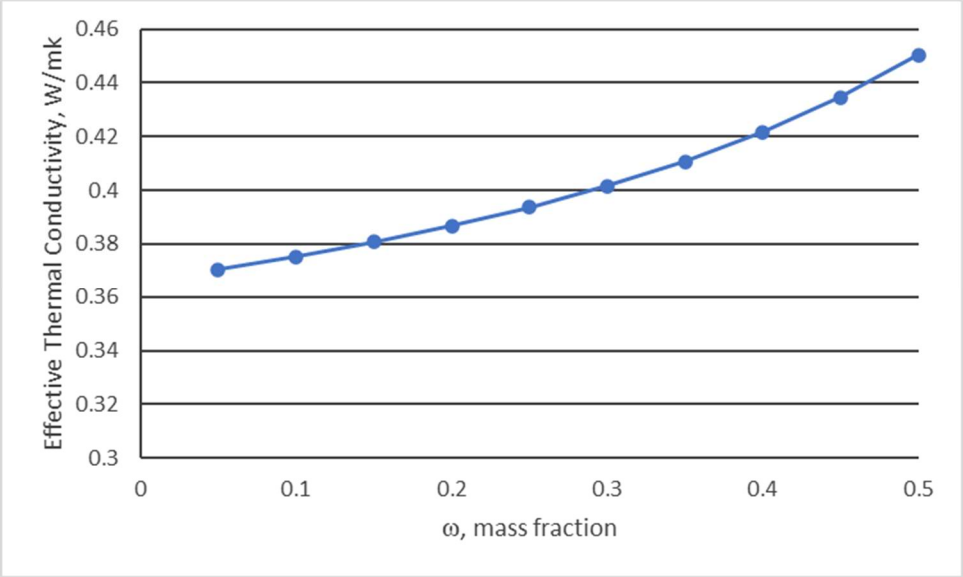

Figure 3.5 k_{eff} vs. ω

Chapter IV. Experimental Investigation

4.1 Experimental Setup

A schematic drawing of the experimental setup is shown in Fig. 4.1. The setup mainly includes a copper OHP, an evaporator, a DC power supply, a condenser, a cooling bath, insulation material, a data acquisition system, a computer, and thermocouples. The DC power supply is connected to the cartridge heaters and supplies the power input to the OHPs. The condenser is made from a 115 × 37 mm^2 aluminum block and is connected to a cooling bath that pumps water at a constant temperature of 15 °C. The evaporator is made from a 50 × 59 mm^2 aluminum block with four cartridge heaters inserted inside. The evaporator and condenser are fastened to the OHP with bolts, with a thin film of OMEGATHERM™201 silicone grease applied between the surfaces to reduce thermal resistance. The total length of the OHP channel is 107 mm, with an evaporator section length of 59 mm, an adiabatic section length of 10 mm, and a condensation section length of 38 mm. As seen in Fig. 4.2, the OHP is fabricated from a 130×80×10 mm copper block with a 3 × 3 mm^2 cross-section channel machined into it. The OHP, shown in Fig. 4.3, is bolted onto a transparent polycarbonate cover plate, with a 0.5 mm thick high-temperature silicone rubber sheet lying between. Insulation material covers the entire back and sides of the OHP to mitigate heat loss to the outside environment.

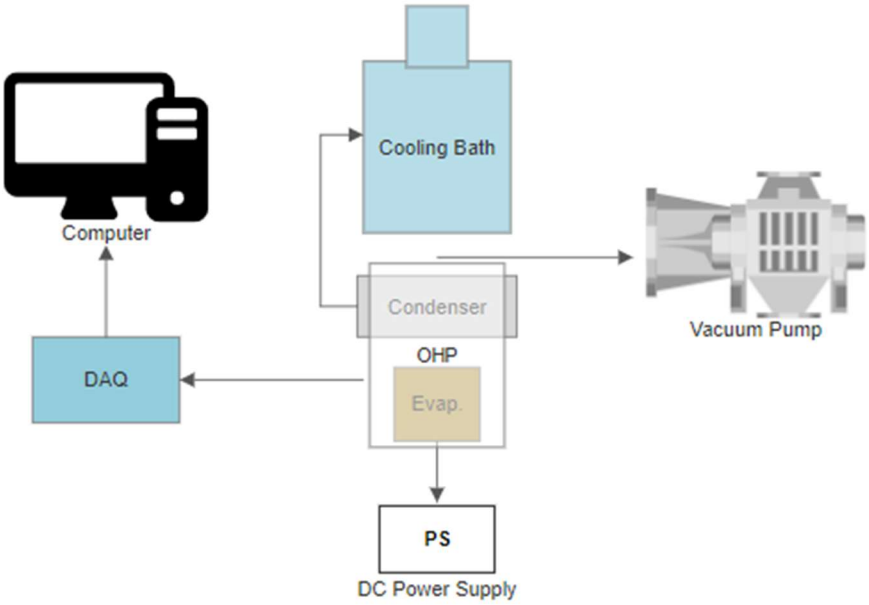

Figure 4.1 Schematic drawing of experimental setup

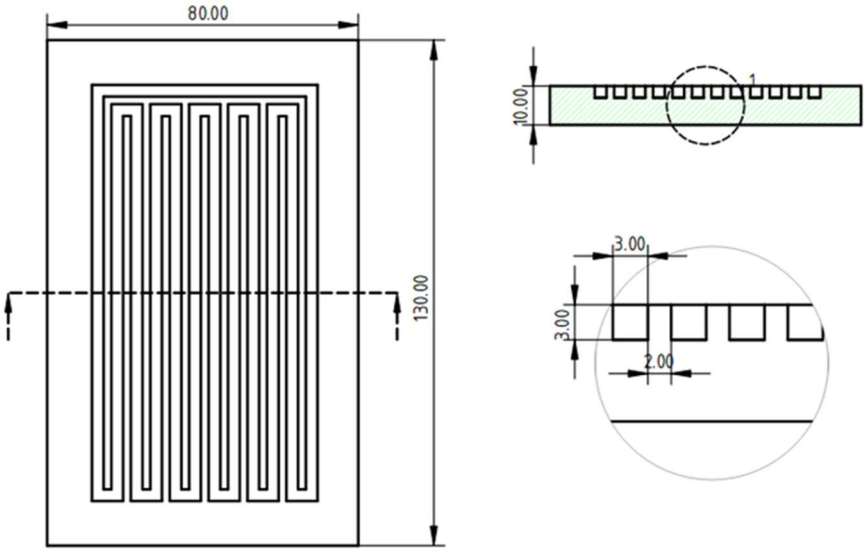

Figure 4.2 Dimensional drawing of OHP

The OHP is evacuated before it is charged using a Varian DS 602 vacuum pump. After a pressure of ~3 × 10^{-1} torr is achieved, the OHP is fully charged with water and then boiled out to ensure minimal air is left in the OHP. The OHP is then charged to a 50% fill ratio with varying concentrations of ethanol-in-gallium hybrid fluid emulsion. The gallium

concentrations by weight fractions are 1%, 5%, 10%, and 20%. Eight T-type thermocouples are implemented into the system to track the temperature. Six thermocouples are inserted into the OHP thermocouple holes to measure the temperature variations: two in the condenser section, two in the adiabatic section, and two in the evaporator section. The remaining two thermocouples are inserted into the inlet and outlet of the condenser block. The temperature data is collected by a Measurement Computing™ USB-2408 at a rate of 5 Hz. The heating input varies from 100 W to 300 W with 50 W increments. The thermal resistance of the OHP is calculated by

$$R = \frac{\overline{T}_e - \overline{T}_c}{Q_e} \tag{4.1.1}$$

where Q_e is the power input into the evaporator via the cartridge heaters, T_e is the area-averaged temperature of the evaporator, and T_c is the area-averaged temperature of the condenser, which can be found by

$$\overline{T} = \frac{\sum_{i=1}^{2} T_i}{2} \tag{4.1.2}$$

The uncertainty of the heat input and the thermal resistance can be calculated by

$$\frac{\delta Q}{Q_e} = \sqrt{\left(\frac{\delta U}{U}\right)^2 + \left(\frac{\delta I}{I}\right)^2} + \frac{\delta Q_{loss}}{Q_e} \tag{4.1.3}$$

$$\frac{\delta R}{R} = \sqrt{\left(\frac{\delta T_e}{T_e - T_c}\right)^2 + \left(\frac{\delta T_c}{T_e - T_c}\right)^2 + \left(\frac{\delta Q}{Q_e}\right)^2} \tag{4.1.4}$$

where U is the voltage output from the DC power supply, and I is the current.

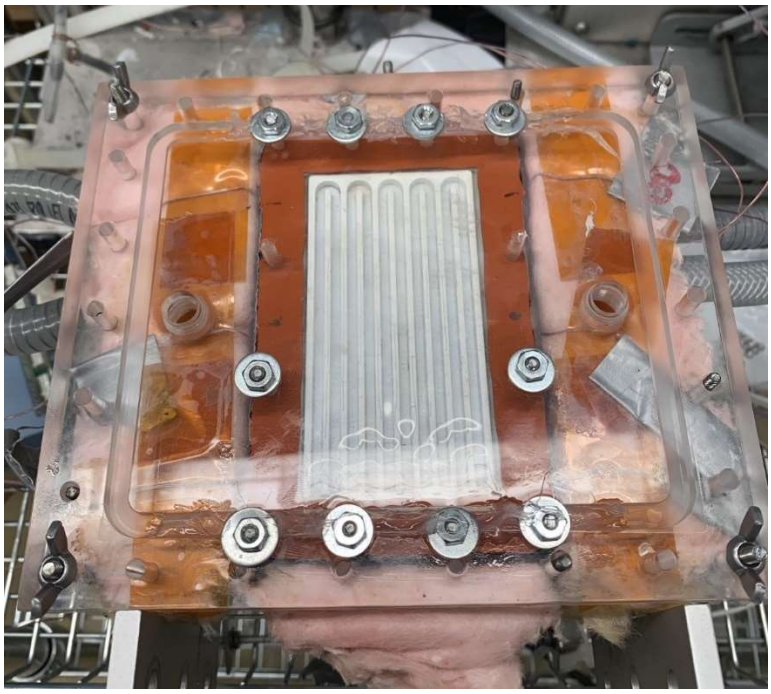

Figure 4.3 OHP

4.2 Results and Discussion

Using the experimental setup described above, the OHP charged with weight concentrations of gallium of 1.0%, 5.0%, 10.0%, and 20.0% was tested. The OHP was able to start up at a minimum heat input of 100 W when charged with ethanol and the various concentrations of hybrid fluids. Vapor nucleation began at the walls of the evaporator section of the OHP. The vapor bubbles then grew larger and began to detach from the wall. A stream of small vapor bubbles would rise from the evaporator section with increasing frequency and begin to grow until distinct vapor plugs and liquid slugs were formed, and oscillation began, as seen in Fig. 4.4. No dry out was observed.

Figure 4.4 Liquid slugs and vapor plugs in OHP channel

Temperature data from the thermocouples distributed across the evaporator, adiabatic, and condenser sections of the OHP was collected and compiled. Figures 4.5-4.9 show the transient temperature responses the OHP charged with the various concentrations of gallium throughout the duration of testing. The OHP exhibited the same behavior for each working fluid tested, an initial rise in temperature at each heat input until a steady state temperature was reached. Using Eqs. (4.1.1) - (4.1.6), the average temperature

difference between the evaporator and condenser, ΔT, the thermal resistance, R, and the effective thermal conductivity, k_{eff}, were calculated.

To calculate the effective thermal conductivity more accurately, heat losses to the environment were considered. Heat transfer from the evaporator to the condenser occurs via conduction through the copper base of the OHP, and through convection and phase-change through the working fluid. Operating an uncharged OHP under the conditions defined for the experiment, heat transfer will only occur through conduction through the copper base. Equation 4.1.5 calculates the heat input of an uncharged OHP using Fourier's law, where ∂T/∂x is the temperature gradient across the OHP.

$$Q = -k_{Cu} A \frac{\partial T}{\partial x} \tag{4.1.5}$$

The calculated heat flux is the true amount of heat that enters the OHP. Table 4.1 shows the heat input, the real heat input, and the percent heat loss to the environment. Using the real heat input, $Q_{e,real}$, the effective thermal conductivity can then be calculated by rearranging Fourier's Law to solve for k

$$k_{eff} = \frac{Q_{e,real} L_{eff}}{A \Delta T} \tag{4.1.6}$$

Table 4.1 Heat input, real heat input, and percent heat loss

Q_e	**$Q_{e,real}$**	**% Heat Loss**
100	85.81	14.19
150	135.90	9.40
200	183.24	8.38
250	229.91	8.04
300	276.91	7.70

The results are shown in Table 4.2. In Figs. 4.10 and 4.11, one can clearly see the divergence of ΔT between ethanol and the different emulsions at a heat input of 250 W and above. At a 300 W heat input, the OHP charged with the 5% wt. gallium-in-ethanol sees the largest drop in ΔT, approximately 3 °C, when compared with the control OHP charged with ethanol. Below 250 W, the temperature difference between the evaporator and condenser shows little to no dependence on the gallium concentration of the emulsion being used. Since all other variables calculated are a function of ΔT, this trend is consistently seen in their outputs as well.

Table 4.2 Average temperature difference, thermal resistance, thermal conductance, and effective thermal conductivity of the OHP

Weight Concentration		0% (Ethanol)	1%	5%	10%	20%
Mass of Gallium [g]		0	0.0048	0.25	0.52	1.14
Effective Density [kg·m^{-3}]		789.2	796.1	824.9	864.1	954.6
Q_e [W]	**Variables**					
100	ΔT [°C]	20.52	20.43	20.44	20.40	20.25
	R [°C /W]	0.205	0.204	0.204	0.204	0.203
	k_{eff} [W/m-°C]	428	430	429	430	433
150	ΔT [°C]	27.79	28.06	27.23	27.36	27.63
	R [°C /W]	0.185	0.187	0.181	0.182	0.184
	k_{eff} [W/m-°C]	500	496	511	508	503
200	ΔT [°C]	33.13	33.45	32.90	32.58	33.22
	R [°C /W]	0.166	0.167	0.164	0.163	0.166
	k_{eff} [W/m-°C]	566	560	570	575	564
250	ΔT [°C]	38.14	38.06	37.26	37.68	38.18
	R [°C /W]	0.152	0.152	0.149	0.151	0.153
	k_{eff} [W/m-°C]	617	618	631	624	616
300	ΔT [°C]	41.55	40.81	38.55	40.09	40.00
	R [°C /W]	0.138	0.136	0.128	0.134	0.133
	k_{eff} [W/m-°C]	682	694	735	707	708

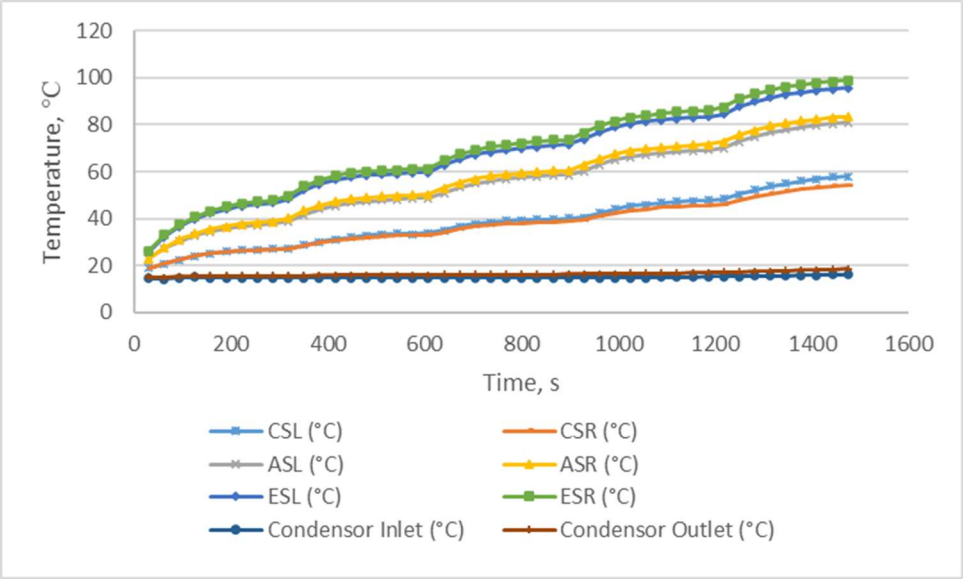

Figure 4.5 Temperature vs. time – pure ethanol

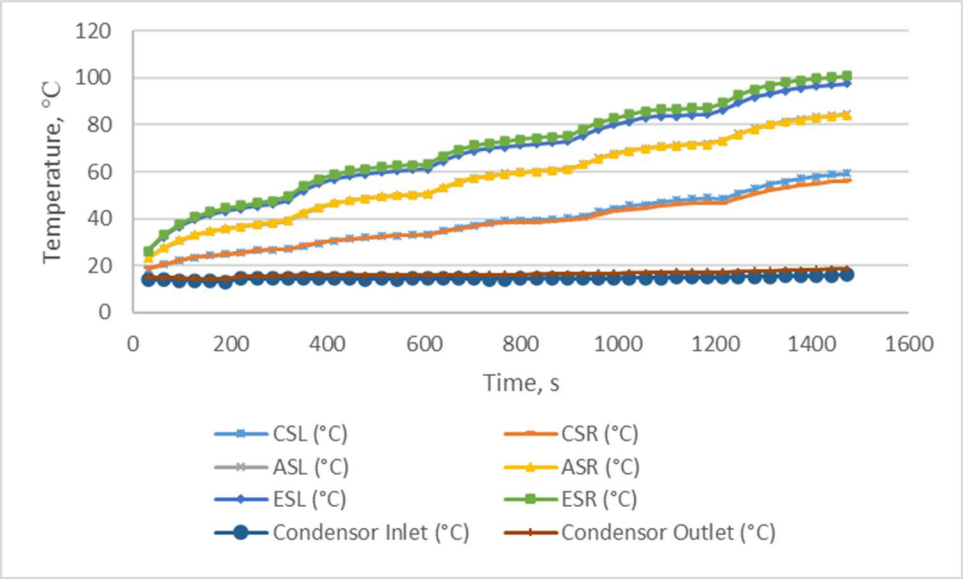

Figure 4.6 Temperature vs. time - 1% wt. gallium-in-ethanol emulsion

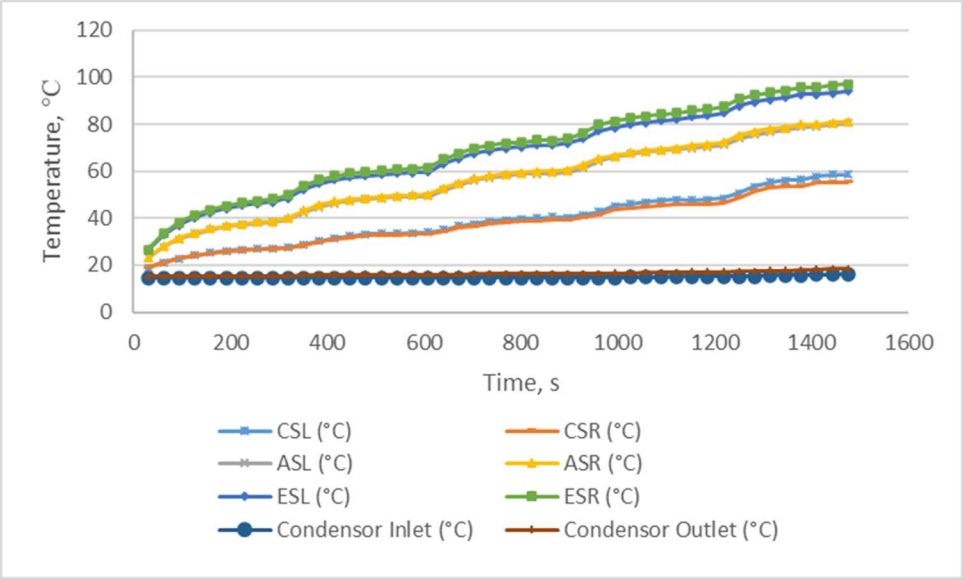

Figure 4.7 Temperature vs. time – 5% wt. gallium-in-ethanol emulsion

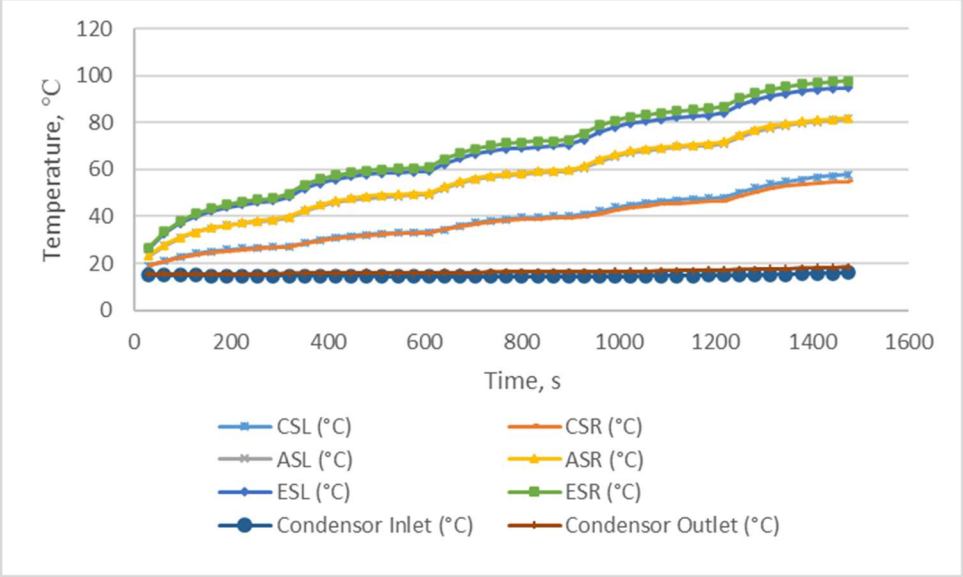

Figure 4.8 Temperature vs. time – 10% wt. gallium-in-ethanol emulsion

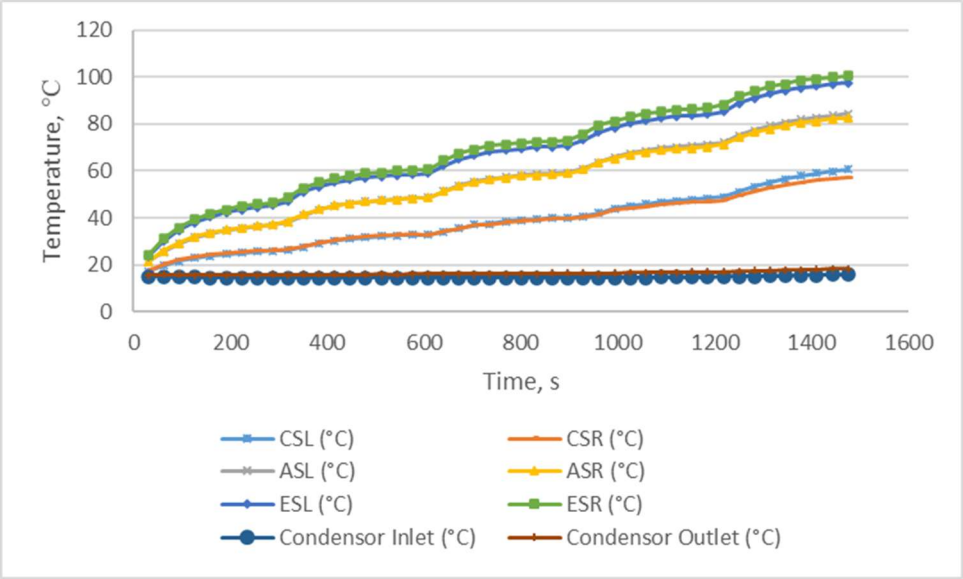

Figure 4.9 Temperature vs. time – 20% wt. gallium-in-ethanol emulsion

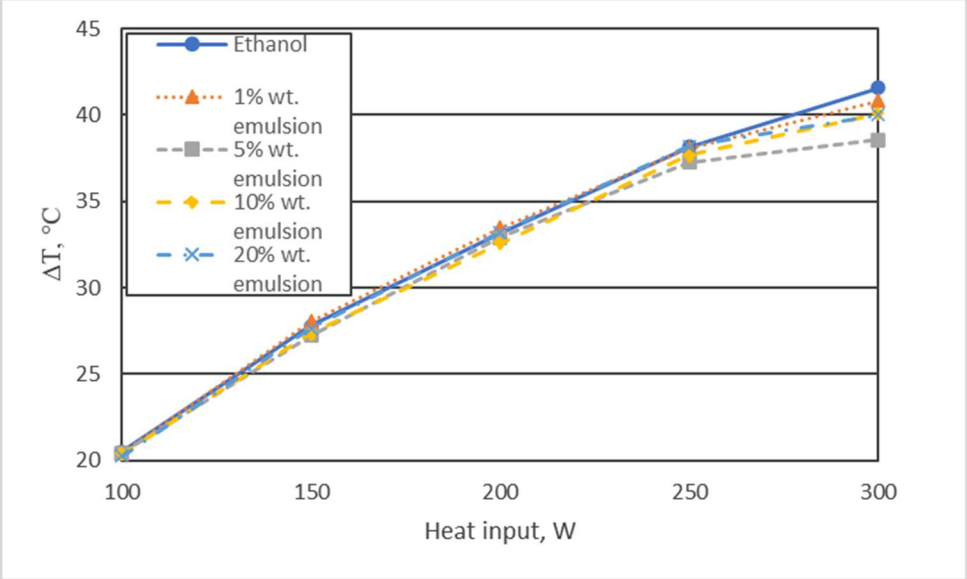

Figure 4.10 ΔT vs. heat input

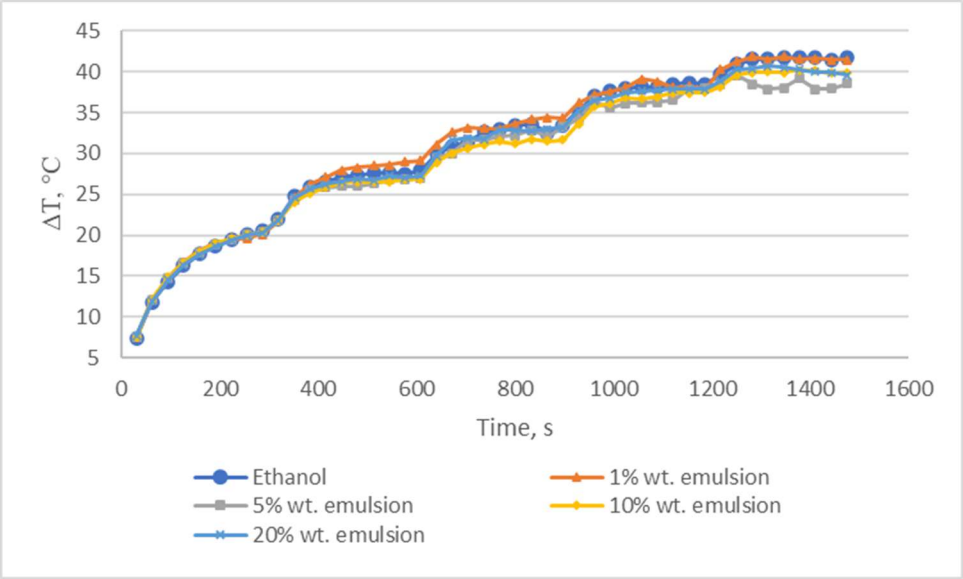

Figure 4.11 ΔT vs. time

Figsures 4.12 and 4.13 show the calculated effective thermal conductivity, k_{eff}, with respect to the heat input. It is observed that a linear relationship between the thermal conductance and power input occurs under 250W, which then diverges as the heat input approached 300 W. Between 250 and 300 W, the OHP charged with the various emulsions begins to noticeably outperform the OHP charged with ethanol. At 300 W, the 5% gallium-in-ethanol emulsion performs the best, resulting in the OHP attaining an effective thermal conductivity of 735 W/m-°C. The 10% and 20% wt. gallium-in-ethanol emulsions perform similarly, showing the next highest effective thermal conductivity of 707 W/m-°C and 708 W/m-°C respectively. The 1% wt. gallium-in-ethanol emulsion shows the least improvement in heat transfer over the control, with an effective thermal conductivity of 694 W/m-°C.

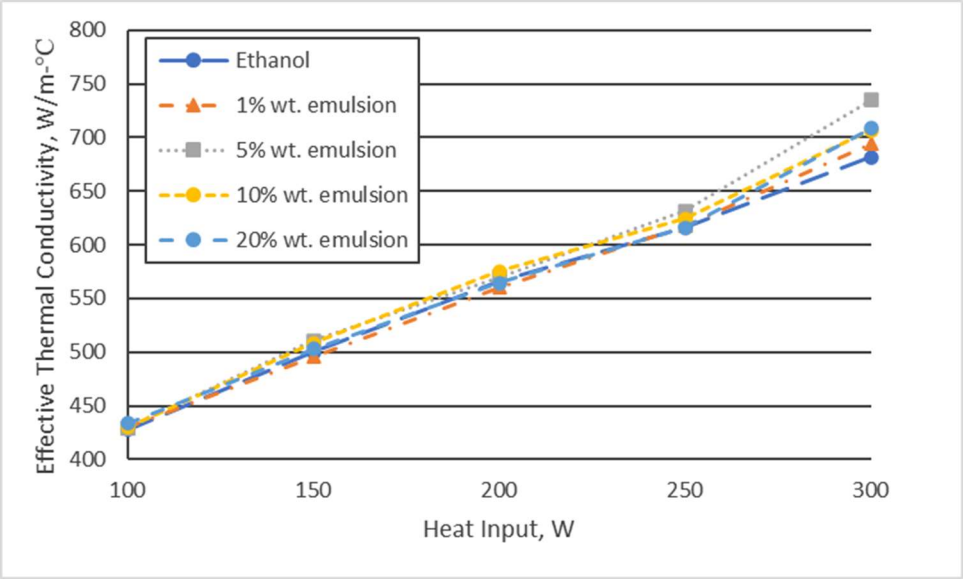

Figure 4.12 Effective thermal conductivity vs. heat input

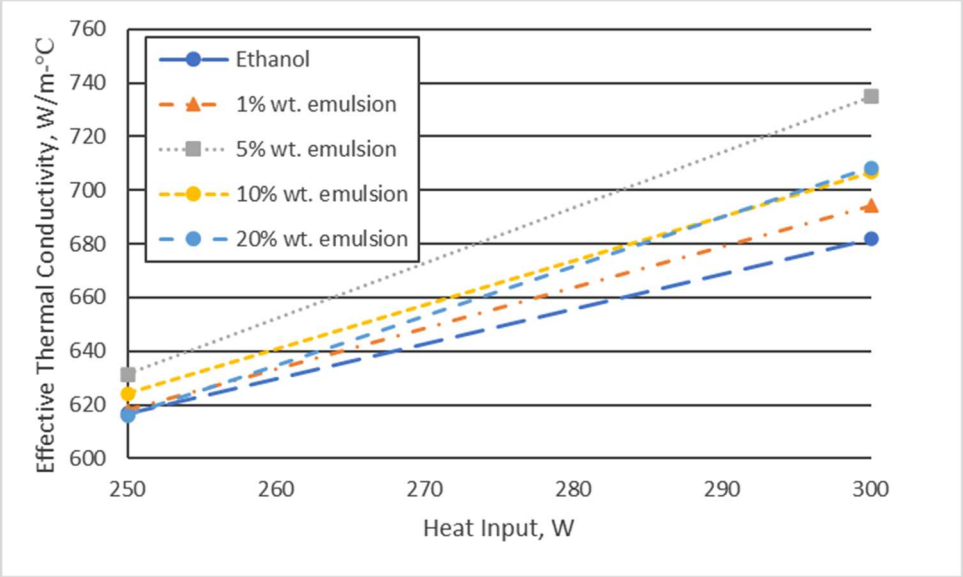

Figure 4.13 Effective thermal conductivity vs. heat input (250-300 W)

Table 4.3 Percent change in effective thermal conductivity compared with ethanol control

Q_e [W]	**0% wt. (Ethanol)**	**1% wt.**	**5% wt.**	**10% wt.**	**20% wt.**
100	0.00%	0.42%	0.38%	0.56%	1.30%
150	0.00%	-0.95%	2.06%	1.59%	0.59%
200	0.00%	-0.95%	0.71%	1.70%	-0.27%
250	0.00%	0.20%	2.37%	1.21%	-0.10%
300	0.00%	1.82%	7.78%	3.63%	3.89%

Table 4.3 shows the percent change in thermal conductivity of the OHPs charged with the emulsions compared to pure ethanol. At 100W, there is a slight positive correlation between the gallium weight concentration and heat transfer improvement, with the 20% wt. concentration performing the best and increasing the thermal conductance by 1.30%. Between 250-300 W, the 5% wt. gallium-in-ethanol emulsion produced an increase in heat transfer of 2.37-7.78% over pure ethanol. The 5% and 10% concentrations improved the heat transfer performance of the OHP across all heat inputs, as opposed to the 1% and 20% concentrations, which saw a reduction in thermal conductance between 150-200 W and 200-250 W respectively.

Chapter V. Conclusions

A numerical and experimental investigation of a hybrid fluid oscillating heat pipe charged with gallium-in-ethanol emulsions was conducted to study the effects on its heat transfer performance. A numerical model of the OHP was created using the VOF method in Ansys Fluent in order to gain a better understanding of the complex two-phase flow dynamics, mass transfer, and heat transfer properties of the OHP under various operating conditions. The numerical model was successfully able to simulate multiple complex flow regimes found in OHPs, including alternating vapor plug and liquid slug flow and bubbly flow. The simulation results showed that using an emulsion of gallium and ethanol as the working fluid improved the heat transfer performance of the OHP compared to using pure ethanol. Introducing the gallium-ethanol emulsion as the working fluid roughly doubled the heat transfer coefficient over using ethanol across all temperature differences. At ΔT= 20 °C, the model showed that the 5% wt. gallium-in-ethanol performed the best, with a heat transfer coefficient of 3200 W/m^2-K. However, no significant correlation was found between the gallium mass concentration and the heat transfer coefficient at ΔT= 30 °C and ΔT= 40 °C.

An emulsion technique, called ultrasonication, was utilized to produce varying concentrations of gallium microdroplets in an ethanol solution for use in the experimental investigation. Four concentrations of gallium-in-ethanol emulsion were fabricated and tested against a control of pure ethanol: 1%, 5%, 10%, and 20%. Between 250-300 W, all the concentrations of gallium-in-ethanol emulsion enhanced the heat transfer capability of the OHP over pure ethanol. The 5% wt. gallium-in-ethanol was found to perform the best, increasing the effective thermal conductivity by 2.42-7.78%. Through the development of

an emulsion-based hybrid fluid, the quantity of gallium needed to reproduce similar heat transfer increases versus previous investigations was drastically reduced, with only 0.25 g of gallium needed to produce a 7.78% increase in heat transfer. Further research into the gravity effect, the skin friction effect, is needed to understand the potential reasons to why a reduction in heat transfer performance occurs when the gallium microparticles of the emulsion are increased to beyond a 5% wt. concentration.

The experimental results verified the model's prediction that the implementation of a gallium-in-ethanol emulsion-based hybrid fluid would improve an OHP's heat transfer performance. However, the model differed from the actual effective thermal conductivity of the OHP by between 4 and 78% with an average uncertainty of 32%. The model also found a smaller effect of ΔT on the heat transfer performance than the experimental investigation. The error found in the simulation results is mainly driven by (1) the uncertainties inherent in using the effective properties of a hybrid fluid, such as the correlation for k_{eff}, instead of the computationally intensive task of modelling individual microparticles in a medium and (2) the inability of the built-in wall function heat transfer coefficient option in Fluent to capture the heat transfer due to phase change.

The potential implications of this research are numerous. The non-chemical enhancement of fluids such as ethanol, that would otherwise not be sufficient in transferring heat, with the implementation of liquid metal microparticles could be promising in both improving the performance of OHPs and cutting down on the costs of production. Further improvement in the modelling of microparticles dispersed in liquid mediums could allow for highly accurate predictions of HFOHP performance, reducing the need for costly and timely lab experimentation.

References

[1] Akachi, H., 1996, "Pulsating heat pipes", *Proceedings 5th International Heat Pipe Symp*.

[2] Akachi, H., 1990, "Structure of heat pipe." U.S Patent 4921041.

[3] Ma, H., 2015, *Oscillating Heat Pipes*, Springer, New York, NY.

[4] Hao, T., Ma, H., and Ma, X., 2019, "Heat transfer performance of polytetrafluoroethylene oscillating heat pipe with water, ethanol, and acetone as working fluids," International Journal of Heat and Mass Transfer, **131**, pp. 109-120.

[5] Hao, T., Ma, X., and Lan, Z., 2017, "Effects of Hydrophilic and Hydrophobic Surfaces on Start-Up Performance of an Oscillating Heat Pipe," Journal of Heat Transfer, **140**(1): 012002.

[6] Hao, T., Ma, X., Lan, Z., Li, N., and Zhao, Y., 2014, "Effects of superhydrophobic and superhydrophilic surfaces on heat transfer and oscillating motion of an oscillating heat pipe", Journal of Heat Transfer, **136**(8): 082001.

[7] Hao, T., Ma, H., and Ma, X., 2019, "Experimental Investigation of a Three-Phase Oscillating Heat Pipe", Journal of Thermal Science and Engineering Applications, **11**(6): 061006

[8] Liu, X., Chen, Y., and Shi, M., 2013, "Dynamic performance analysis on start-up of closed-loop pulsating heat pipes (CLPHPs)", International Journal of Thermal Sciences, **65,** pp. 224-233.

[9] Cheng, P., and Ma, H., 2011, "A Mathematical Model of an Oscillating Heat Pipe", Heat Transfer Engineering, **32**(11-12), pp. 1037-1046.

[10] Liu, J., and Zhou, X., 2002, "A computer chip cooling method which uses low melting point metal and its alloys as the cooling fluid." China Patent 2131419.

[11] Ma, K., and Liu, J., 2007, “Liquid metal cooling in thermal management of computer chips”, Frontiers in Energy, **1**, pp. 384–402.

[12] Hao, T., Ma, H., and Ma, X., 2019, “Experimental investigation of oscillating heat pipe with hybrid fluids of liquid metal and water”, Journal of Heat Transfer, **141**(7): 071802.

[13] Ma, H., Wilson, C., Yu, Q., Park, K., Choi, U., and Tirumala, M., 2006, “An experimental investigation of heat transport capability in a nanofluid oscillating heat pipe”, Journal of Heat Transfer, **128**(11), pp. 1213-1216.

[14] Ji, Y., Wilson, C., Chen, H., and Ma, H., 2011, “Particle shape effect on heat transfer performance in an oscillating heat pipe”, Nanoscale Research Letters, **6**.

[15] Kumano, H., Hiroi, K., and Asaoka, T., 2017, “Experimental study on flow and heat transfer characteristics of oil/water emulsions: part ii – heat transfer characteristics”, Applied Thermal Engineering, **127**, pp. 1555-1563.

[16] Trinh, V., and Xu, J., 2017, “An experimental study on flow and heat transfer characteristics of ethanol/polyalphaolefin nanoemulsion flowing through circular minichannels”, Nanoscale Research Letters, **12**.

[17] Smoot, C., and Ma, H., 2017, "Numerical Analysis of a Vapor Bubble Oscillating in a Capillary Channel" Journal of Thermophysics and Heat Transfer **31**(1), pp. 154-164.

[18] Taha, T., and Cui, Z., 2004 “Hydrodynamics of slug flow inside capillaries” Chemical Engineering Science, **59**(6), pp. 1181-1190.

[19] Liu, X., and Yingli, H., 2009 "Numerical simulation of vapor-liquid two-phase flow in a closed loop oscillating heat pipe" ASME International Mechanical Engineering Congress and Exposition, **43826**, pp. 609-617.

[20] Krupiczka, R., 1967, "Analysis of thermal conductivity in granular materials" International Chemical Engineering **7**(1): 122-+.

[21] Zhang, Y., Tang, S., Zhao, Q., Yun, G., Yuan, D., and Li, W., 2019, "High-throughput production of uniformly sized liquid metal microdroplets using submerged electrodispersion", Applied Physics Letters, **114**(15): 154101.

[22] Hutter, T., Elliott, S., Huck, W., and Bauer, W., 2012, "Formation of Spherical and Non-Spherical Eutectic Gallium-Indium Liquid-Metal Microdroplets in Microfluidic Channels at Room Temperature", Advanced Functional Materials, **22**(12), pp. 2624-2631.

[23] Huang, C., Zong, J., Wang, X., Cao, Q., Zhang, D., and Jiang, J., 2021, "Production of Uniformly Sized Gallium-Based Liquid Alloy Nanodroplets via Ultrasonic Method and Their Li-Ion Storage", Materials, **14**(7): 1759.